Acta Crystallographica Section D
Biological Crystallography
ISSN 0907-4449

Three-dimensional structures of a humanized anti-IFN-γ Fab (HuZAF) in two crystal forms

Philip C. Bourne,[a] Simon S. Terzyan,[b] Gwendolyn Cloud,[b] Nicholas F. Landolfi,[c] Maximiliano Vásquez[c] and Allen B. Edmundson[b]*

[a]Department of Veterinary Pathobiology, Oklahoma State University, Stillwater, OK 74078-2007, USA, [b]Crystallography Program, Oklahoma Medical Research Foundation, 825 Northeast 13th Street, Oklahoma City, OK 73104, USA, and [c]Protein Design Labs Inc., 34801 Campus Drive, Fremont, CA 94555, USA

Correspondence e-mail: allen-edmundson@omrf.ouhsc.edu

Received 6 April 2004
Accepted 29 July 2004

PDB References: humanized anti-IFN-γ Fab, orthorhombic $P2_12_12_1$ form, 1t3f, r1t3fsf; monoclinic $C2$ form, 1t04, r1t04sf.

Three-dimensional structures were determined for two crystal forms (orthorhombic $P2_12_12_1$ and monoclinic $C2$) of the Fab from the humanized version of a murine monoclonal antibody (AF2) that possesses binding and potent neutralizing activity against human interferon γ (IFN-γ). This humanized antibody (HuZAF; USAN name fontolizumab) is currently in phase II clinical trials for the treatment of Crohn's disease. HuZAF exhibits binding and IFN-γ neutralizing capacities that closely approximate those of the original antibody. It is shown that HuZAF, whose VH domain was designed using a best-sequence-fit approach, is closer structurally to its mouse precursor than is a version whose VH was constructed using a human sequence with lower homology to the original mouse sequence. This work thus offers direct structural evidence in support of the best-sequence-fit approach and adds to previous results of biological and biochemical evaluations of distinctly engineered antibodies that also favored the use of a best-sequence-fit strategy. A second crystal type appeared during attempts to crystallize the Fab–IFN-γ complex. The antibody–antigen complex that existed in solution dissociated in the crystallization mixture. A conformationally altered but unliganded HuZAF protein crystallized in a different space group ($C2$), with two Fab molecules in the asymmetric unit. In this crystal lattice, no space was available for accommodating the IFN-γ antigen. Thus, there are currently three slightly different structures of the HuZAF Fab.

1. Introduction

There has been increasing interest in the development of antibodies for the treatment of many human diseases (Johnson *et al.*, 1997; Maloney *et al.*, 1997; Vincenti *et al.*, 1998; Waldmann, 1991). Mice have commonly been used to produce monoclonal antibodies (mAbs) with the required specificity for appropriate targets. Mice are easy to immunize, tend to show little or no tolerance to human antigens and produce B cells that can be fused with a myeloma partner to generate stable hybridomas that secrete large quantities of the desired antibody. However, murine MAbs are immunogenic in humans. To address this practical shortcoming, chimeric antibodies with murine V and human C domains were constructed to lessen but not eliminate the immunogenicity (Boulianne *et al.*, 1984; Morrison *et al.*, 1984).

The next stage of development was the introduction of humanized therapeutic antibodies (Queen *et al.*, 1989; Riechmann *et al.*, 1988) produced by grafting 'donor' rodent complementarity-determining regions (CDRs) onto 'acceptor' human framework regions (FRs). Humanization procedures substantially reduce the 'foreign' content and the attendant

immunogenic side effects of Ab therapeutic agents (Vincenti *et al.*, 1998). Additional framework changes are found to be necessary to restore the complete antigen-binding activity and functionality of the starting mouse antibody. Detailed knowledge of the three-dimensional structure of a murine antibody can promote rational decisions as to which residues may have functional implications and should be retained in the humanized version. Such structures have often been predicted by comparative modeling procedures (Carter *et al.*, 1992; Queen *et al.*, 1989; Zilber *et al.*, 1990) with relative success, but access to high-resolution atomic structures is clearly preferable.

Human γ-interferon (IFN-γ) is a key cytokine involved in the development and maintenance of the Th1 arm of the immune system. Elevated levels of IFN-γ occur in response to viruses and other infectious agents and are essential to a successful immune response. Elevated levels of IFN-γ have also been observed in immune-mediated conditions such as Crohn's disease, multiple sclerosis and psoriasis. Thus, this cytokine is considered to be an attractive target for the development of therapeutic antibodies for the treatment of such diseases.

With the intent of developing a humanized therapeutic antibody, a panel of murine monoclonal antibodies directed against human recombinant IFN-γ was generated. The most potent of these was an IgG2b-κ antibody (designated AF2) that neutralized the activity of human IFN-γ by preventing the interaction of IFN-γ with its cellular receptor (Thakur & Landolfi, 1999).

Two sets of humanized AF2 variants were constructed in an effort to obtain a humanized antibody against IFN-γ with optimal binding affinity and biological activity. All variants were constructed using the human Ab Eu sequence (Edelman & Gall, 1969; Gottlieb *et al.*, 1970) as an acceptor framework for the VL domain because of the high degree of homology between the human acceptor-framework sequence and the murine donor-framework sequence; the VL sequence of Eu is 65% identical to the murine AF2 VL sequence. For the VH domain, two different acceptor-framework sequences have been used, the VH subgroup I Eu and the subgroup III Nie (Ponstingl *et al.*, 1970, which are 58 and 48% identical to the murine AF2 VH sequence, respectively. The best variant based on the Nie VH framework sequence, termed HuAF2, had similar binding affinity but was about ten times less potent in neutralization when compared with the murine AF2 or chimeric version of AF2 (ChiAF2). The three-dimensional structure of the HuAF2 Fab has previously been determined (Fan *et al.*, 1999).

The initial variants based on the more homologous Eu VH acceptor framework sequence retained, within about twofold, the affinity of the murine antibody. However, they exhibited a decrease in IFN-γ neutralization of tenfold or more. A systematic generation and evaluation of additional Eu-based AF2 variants was undertaken, leading to the production of a variant, termed HuZAF, which retained both the affinity and neutralization activity of the murine or chimeric versions within about twofold. Such an improvement largely arose from altering the VH framework residue at position 11. A detailed account of this work has been published elsewhere (Landolfi *et al.*, 2001).

The present report is primarily concerned with the crystallographic analysis of the Fab structure of HuZAF. This Fab crystallized in two forms, orthorhombic $P2_12_12_1$ and monoclinic $C2$; the latter has two Fab molecules with slightly different conformations in the asymmetric unit. A comparison of these three new structures of the same Eu-based Fab with those previously determined (Fan *et al.*, 1999) for the chimeric Fab (ChiAF2) and the Nie-based Fab (HuAF2) is also reported here. To our knowledge, this is the first example in the literature of a structural comparison of humanized Fab versions of the same mouse antibody based on distinct choices of human frameworks.

2. Materials and methods

2.1. Preparation of the HuZAF antibody

A humanized anti-interferon-γ antibody (HuZAF) was produced in highly purified form as described elsewhere (Landolfi *et al.*, 2001). In general, the L and H chains were designed to have three complementarity-determining regions (CDRs) from the functional AF2 murine antibody grafted onto human 'framework regions' (FR) of the variable domains (VL and VH), as outlined in §1. 'Constant' (C) regions, making up the remainder of the antibody (CL, CH1, CH2 and CH3 domains and the 'hinge region' between CH1 and CH2), were exclusively of human origin: a κ-type L chain and a γ1 H chain.

2.2. Preparation and crystallization of Fabs

Antigen-binding fragments (Fabs) were prepared by a protocol originally designed for the ChiAF2 protein (Fan *et al.*, 1999). HuZAF antibodies were hydrolyzed with papain (1:50 weight ratio of enzyme to antibody) for 16 h in an ice bath. The enzyme was removed from the reaction mixture by gel filtration at 277 K on a 2.5 $\times$ 100 cm column of Sephacryl S-200, which also separated the Fab component from the Fc and the residual antibody. Further purification was achieved by anion-exchange chromatography of the Fab at 293 K on a 2.5 $\times$ 25 cm column of Whatman DE 52 (DEAE-Cellulose). Crystallization trials were conducted with a standard vapor-diffusion procedure using sitting drops and the Crystal Screen kit from Hampton Research, Laguna Niguel, CA, USA. The protein was dialyzed against deionized water and concentrated to 4 mg ml^{-1}. Droplets containing 3 µl of protein (4 mg ml^{-1}) and 3 µl of 18%(*v*/*v*) PEG 6000 in 100 m*M* sodium citrate pH 5.0 were equilibrated over wells containing 1 ml of 18%(*v*/*v*) PEG 6000 in the same buffer. Crystal plates with dimensions of 0.4 $\times$ 0.3 $\times$ 0.1 mm appeared after one week at 285 K.

2.3. Preparation and crystallization of a complex of the HuZAF Fab with its IFN-γ ligand

This complex was prepared at pH 7–8.5 in 0.02 *M* Tris, 0.15 *M* NaCl by mixing the HuZAF Fab with an IFN-γ dimer in a molar ratio of 2.5:1 (slight excess of HuZAF over IFN-γ). On a 2.5 × 100 cm sizing column of Sephacryl S-200 with the above buffer as eluent, the major component was demonstrated by SDS–PAGE to consist of two molecular quantities of Fab and one of IFN-γ, as expected for a 2:1 complex. A minor component emerging from the column just after the major band was found to contain only unliganded HuZAF Fab.

The major component was dialyzed against deionized water and concentrated to 4 mg ml^{-1} with a Microprodicon membrane. No proteins were found to escape through the membrane. For a crystallization screen at 285 K, 3 µl of the major component (4 mg ml^{-1}) was mixed with 3 µl of 18% PEG 8000, 0.1 *M* $(NH_4)_2SO_4$, 0.01 *M* $MgCl_2$ and 0.05 *M* MES pH 5.6; the reservoir contained 1.0 ml of the same solution. Crystals quite different in appearance from those of the orthorhombic form were produced in one month.

2.4. Collection of X-ray diffraction data

For collection of X-ray data, crystals of the HuZAF Fab were transferred into a cryoprotectant consisting of 22% PEG 6000, 28% PEG 400 and 100 m*M* citrate pH 5. These crystals were flash-cooled in liquid nitrogen and subjected to X-ray analysis with a Rigaku RU-H3R X-ray generator coupled with a MAR345 image-plate detector. The X-ray beam was collimated with Osmic Max-Flux Confocal mirrors. X-ray diffraction data were collected at 100 K to 2.0 Å resolution using one crystal. Data were reduced and scaled with the *HKL* program suite, including *DENZO* and *SCALEPACK* (Otwinowski & Minor, 1997). Similar procedures were employed in the data collection from a crystal of the putative Fab–IFN-γ complex. For cryoprotection, the mother liquor of the crystal was brought to 10%(*v*/*v*) in 2-methyl-2,4-pentanediol (MPD). However, the X-ray data for this crystal only extended to 3.0 Å resolution (Table 1).

2.5. X-ray analysis for the orthorhombic form of the HuZAF Fab

Like its chimeric and HuAF2 predecessors, the HuZAF Fab crystallized in the orthorhombic space group $P2_12_12_1$, with unit-cell parameters a = 64.4, b = 74.3, c = 104.6 Å. The crystal structure was solved by the molecular-replacement method (Fitzgerald, 1988; Rossmann, 1990) with the program *AMoRe* (Navaza, 1994) and the model PDB entry 1b4j (Fan *et al.*, 1999). A clear solution was found with a correlation coefficient of 45.9 (*R* factor of 39.4%). The crystallographic asymmetric unit consisted of one HuZAF Fab with a molecular weight of 46 808 Da; the solvent content of the crystal was 53.6% and the Matthews coefficient, V_M, was 2.7 Å^3 Da^{-1} (Matthews, 1968).

The atomic coordinates of the preliminary model were refined using *REFMAC*5 (Murshudov *et al.*, 1999) and the *CCP*4 suite of programs (Collaborative Computational Project, Number 4, 1994). Iterative model building and substitution of the correct sequences were performed using *O* (Jones *et al.*, 1991). As the conventional *R* factor (R_{cryst}) dropped below 20%, water molecules were placed at stereochemically reasonable positions if they had densities in both $2F_o - F_c$ (1σ) and $F_o - F_c$ (3σ) maps. For the final steps of refinement, 434 protein residues (214 from VL-CL and 220 from VH-CH1) and 383 water molecules were included in the Fab model.

Table 1
Data-collection and refinement statistics.

Data statistics		
Space group	$P2_12_12_1$	$C2$
Molecules in AU	1	2
Unit-cell parameters		
a (Å)	64.39	82.27
b (Å)	74.27	169.80
c (Å)	104.64	72.82
β (°)		97.68
Resolution† (Å)	30.0–2.0 (2.03–2.0)	25.0–3.0 (3.11–3.0)
R_{merge}†	0.055 (0.313)	0.146 (0.387)
No. of reflections†	30615 (1518)	19324 (1914)
Completeness (%)	88.5 (93.0)	97.1 (96.9)
Redundancy	3.0	2.49
$I/\sigma(I)$†	17.9 (3.15)	6.14 (2.27)
Refinement statistics		
R_{work} (%)/No. reflections	17.3/27520	21.7/16839
R_{free} (%)/No. reflections	22.4/1547	29.3/868
No. non-H atoms		
Protein	3299	6602
Solvent	377	47
R.m.s. deviation from ideal values		
Bond lengths (Å)	0.015	0.007
Bond angles (°)	1.55	1.39
Average B factor‡ (Å^2)	29.0 (25.13)	28.29 (51.72)
First molecule		28.25
Second molecule		28.33
Program used	*REFMAC*	*CNS*
Statistics from Ramachandran plot (Laskowski *et al.*, 1993)		
Most favorable regions (%)	89.0	79.6
Additionally allowed regions (%)	9.4	18.5
Generally allowed regions (%)	0.5	1.3
Disallowed regions (%)	1.1	0.5

† Values in parentheses represent corresponding values for the highest resolution shell. ‡ Values in parentheses are the *B* factor estimated from a Wilson plot.

2.6. X-ray analysis of the monoclinic form of the HuZAF Fab

Unlike the native protein, the mixture of HuZAF Fab and IFN-γ produced crystals belonging to the monoclinic $C2$ space group, with unit-cell parameters a = 82.3, b = 169.8, c = 72.8 Å, β = 97.7°. With the orthorhombic form of the HuZAF Fab as the starting model, the structure was solved at 3.0 Å resolution by the molecular-replacement method using the program *AMoRe* (Navaza, 1994). The correlation coefficient and *R* factor were 43.0 and 43.5%, respectively, for the best solution. The crystallographic asymmetric unit was comprised of two Fab molecules (6649 non-H atoms), which occupied approximately 54% of the crystal volume. The most significant finding in the analysis of the putative antigen–antibody complex was the exclusion of the IFN-γ ligand from the crystal lattice. The two Fabs in the asymmetric unit were related by a pseudo-

twofold axis of rotation. The binding sites of both Fabs in the pair were empty and the holes between each pair and symmetry-related molecules were too small to accommodate an IFN-γ antigen. Crystallographic refinement was conducted by the general procedure described above for the unliganded Fab, using the programs *CNS* (Brünger *et al.*, 1998) and *TURBO-FRODO* (Roussel & Cambillau, 1989). Statistics for the refinement of both forms of the HuZAF Fab are summarized in Table 1.

With the program *ROTMOL*, kindly provided by W. Steigemann and R. Huber, sets of residues were excerpted from the most regular portions of the β-pleated sheets and used to calculate the 'elbow-bend' angle for each of the three Fab variants. This is defined as the angle subtended by the pseudodyads between the VH-VL and CH1-CL domain pairs.

Table 2
Comparison of AF2 structures.

The upper triangle contains the r.m.s. deviations (Å) of C^{α} atoms over the entire Fab (429/436 atoms); the lower triangle contains r.m.s. deviations over the V domains only (223 atoms).

	ChiAF2	HuAF2	HuZAF (1)†	HuZAF (2)‡	HuZAF (3)§
ChiAF2	N/A	1.22	0.87	1.00	0.95
HuAF2	1.34	N/A	0.85	0.86	0.95
HuZAF (1)†	0.75	1.23	N/A	1.05	1.05
HuZAF (2)‡	0.89	1.24	0.59	N/A	0.30
HuZAF (3)§	0.90	1.27	0.61	0.19	N/A

† HuZAF structure in the orthorhombic crystal. ‡ HuZAF structure in the monoclinic crystal, first molecule. § HuZAF structure in the monoclinic crystal, second molecule.

3. Results

3.1. Amino-acid sequence of three Fabs: HuZAF, HuAF2 and ChiAF2

The amino-acid sequences of the VL and VH domains from HuZAF, HuAF2 and ChiAF2 Fabs are listed in Fig. 1. The sequence of the HuZAF VL was identical to that of HuAF2 and the three-dimensional structure was initially assumed to be the same. In the HuZAF VH, the sequence changes involved 21 residues in the FRs. Mostly, these substitutions reflected differences between the two FR donor sequences, Eu and Nie, which belong to VH subgroups I and III, respectively, as used in the designs of the HuZAF and HuAF2 humanized Abs. Two of the changes (leucine for valine 11H; lysine for arginine 38H) were based on the functional consequences of mutational studies reported previously (Landolfi *et al.*, 2001).

3.2. Three-dimensional structure of the orthorhombic form of the HuZAF Fab

Statistics for the refinements of both forms of the HuZAF Fab are summarized in Table 1. A stereo diagram of the ribbons model of the HuZAF Fab prepared with the program *MOLSCRIPT* (Kraulis, 1991) is shown in Fig. 2. It has the general features expected for a typical human Fab but differs in detail from the structure of the HuAF2 Fab (PDB code 1b4j) reported previously (Fan *et al.*, 1999). Each domain consists of two antiparallel β-pleated sheets covalently linked by an

```
                10        20        30        40        50        60
HuZAF     DIQMTQSPSI LSASVGDRVT ITCKASENVD TYVSWYQQKP GKAPKLLIYG ASNRYTGVPS
ChiAF2    ..V.....KS MYV.I.E... LS........ .......... EQS....... .........D

                70        80        90       100       108
HuZAF     RFSGSGSGTD FTLTISSLQP DDFATYYCGQ SYNYPFTFGQ GTKVEVKR
ChiAF2    ..T....A.. .......V.A E.L.D.H... .........S ...L.I..

                                   (a)

                10        20        30        40        50        60
HuZAF     ZVQLVQSGAE LKKPGSSVKV SCKASGYIFT SSWINWVKQA PGQGLEWIGR IDPSDGEVHY
HuAF2     ........GG V.Q..R.L.L ..L....... .........R ..R....... ..........
ChiAF2    ....Q.P.AD LVM..APV.L ..L....... .........R ..R....... ..........

                70        80        90       100       110      117
HuZAF     NQDFKDKATL TVDKSTNTAY MELSSLRSED TAVYYCARGF LPWFADWGQG TLVTVSS
HuAF2     ......RF.I SR...K..L. L.MN...P.. .......... .......... .......
ChiAF2    .......... .....SS.A. IQLN..TS.. S......... .......... ......A

                                   (b)
```

Figure 1
Amino-acid sequences of (*a*) the VL and (*b*) the VH domains of the HuZAF, HuAF2 and ChiAF2 antibodies. VL domains of the humanized HuZAF and HuAF2 variants have identical sequences based on murine AF2 CDRs and human Eu framework (FR) sequences. VH domains were constructed with different FRs: HuZAF from the subgroup I Eu sequence and HuAF2 from the subgroup III Nie sequence. The ChiAF2 sequences refer to the murine components in a chimeric antibody with AF2 V domains and human C domains (κ_1 and γ_1 isotypes).

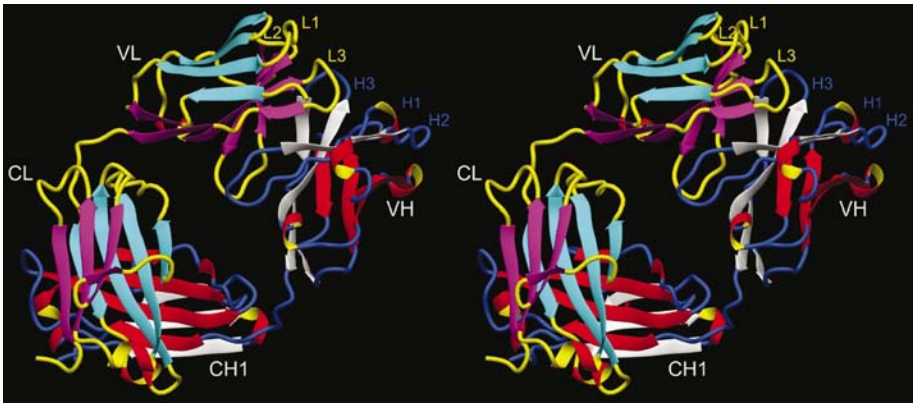

Figure 2
Stereo illustration of the three-dimensional structure of the HuZAF Fab, prepared with the program *MOLSCRIPT* (Kraulis, 1991). Secondary elements are superimposed on backbone tracings, which are colored yellow in the L chain and steel blue in the H chain. β-Strands are represented by directional arrows: cyan for the four-stranded β-pleated sheets and magenta for the five-stranded (VL) and three-stranded layers (CL) of the L chain and red and white for the corresponding β-pleated sheets in the H chain. Helices are identified by red and yellow spirals. CDRs are marked 1, 2 and 3.

intra-chain disulfide bond. The antigen-binding site, consisting of six CDRs, three from each chain, dominated surfaces at the tip of the Fab. As shown in Fig. 1, the amino-acid sequences of these CDRs were identical to those in the original murine monoclonal antibody or the ChiAF2 Fab (PDB code 1b2w). When the three-dimensional structures of the CDRs in the HuZAF Fab were compared one by one with their murine counterparts in the ChiAF2 Fab, their conformations were almost completely superimposable. The r.m.s. deviations among the five Fab conformations, the three reported here for HuZAF and the chimeric and HuAF2 versions described previously, are summarized in Table 2. The C^{α} traces of the VL-VH match with an optimal r.m.s. deviation of 0.75 Å; for the VL and VH individually, the r.m.s. deviations are 0.55 and 0.85 Å, respectively. This figure is 0.78 Å for all CDRs, 0.48 Å for the CDRs of VL and 0.94 Å for the CDRs of VH.

The 'elbow-bend' angles were calculated to be 166.6° for the ChiAF2 Fab, 167.5° for the HuAF2 Fab and 177.6° for the HuZAF Fab. In the *C*2 form, the two HuZAF elbow-bend angles of the two HuZAF Fab variants were 170.2 and 171.9°, respectively.

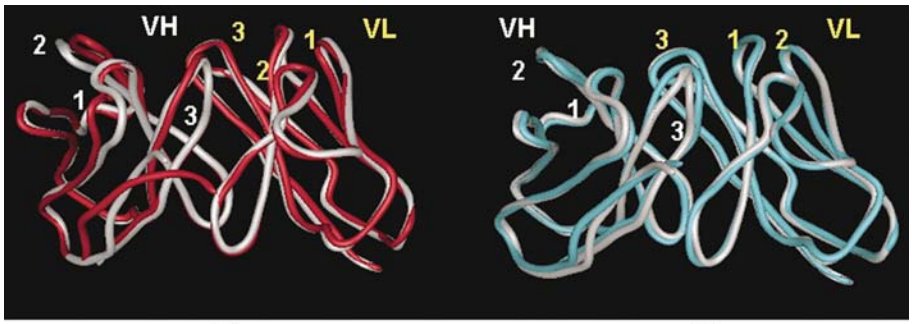

Figure 3
(*a*) Polypeptide tracings of the VH and VL domains of the HuAF2 Fab (PDB code 1b4j) in red, superimposed on those of the murine domains in the mouse–human chimeric ChiAF2 Fab (PDB code 1b2w) in white. CDRs in the HuAF2 have amino-acid sequences excerpted from those in the original murine AF2 antibody. (*b*) Backbone tracings of HuZAF V domains (cyan) overlaid on those of ChiAF2 (Maloney *et al.*, 1997). In HuZAF, the substitution of two acceptor framework residues with mouse residues, Val11 by leucine and Arg38 by lysine, significantly improves the structural mimicry relative to ChiAF2.

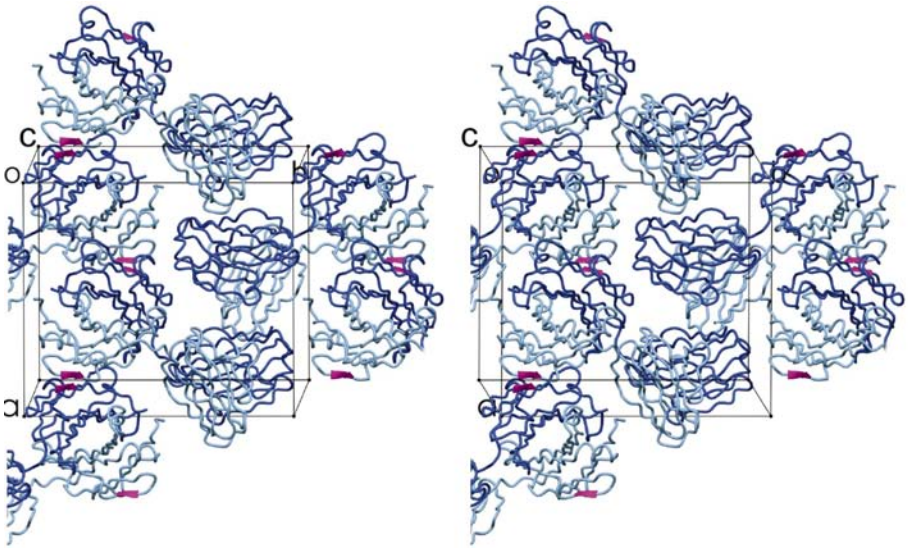

Figure 4
Stereo diagram of the crystal packing of the HuZAF Fab in the orthorhombic $P2_12_12_1$ space group, with one Fab as the crystallographic asymmetric unit. The L chain is colored sky blue and the H chain royal blue. CL and CH1 domains can be identified by the pink directional arrows. These arrows indicate the outermost β-strands in symmetry-related molecules: residues 159–163 from the four-stranded β-pleated sheet of the L chain (designated 4–4) and residues 209–214 (3–3) from the three-stranded layer of the H chain. Cross-molecule β-strand pairing is mediated by the formation of four hydrogen bonds between appropriate carbonyl O and amido H atoms of the parallel backbone segments of L4–4 in the uppermost Fab and H3–3 in the Fab below it. On the underside of the latter Fab, the hydrogen-bonding pattern is duplicated in reverse between L4–4 and the H3–3 of a third Fab molecule. Together, the stacking interactions lead to a vertical ribbon (along *c*) of molecules of indefinite length in the crystal lattice. This type of packing is unusual because two dissimilar antiparallel β-pleated sheets on different molecules are joined by parallel β-strand pairing across a twofold axis. VL-VH modules protrude from alternating sides of the vertical column of CL and CH1 domains but contribute less substantially to the crystal packing. Their participation is restricted mainly to spatial complementarity.

3.3. Comparisons of the V domains of the chimeric AF2 with those of HuAF2 and HuZAF

Stereo diagrams of superimposed variable domains (VH and VL) are presented in Fig. 3 and r.m.s. deviation-based comparisons are presented in in Table 2. The first panel of Fig. 3 compares the V domains of the HuAF2 antibody with those of the chimeric version, ChiAF2, and the second panel depicts a similar overlay of the HuZAF and ChiAF2 V domains.

Both diagrams clearly indicate that the VL domains of the two humanized antibodies conformed very closely to the structure of the chimeric molecule; the r.m.s. deviations for the C^{α} atoms are 0.55 and 0.60 Å when comparing ChiAF2 to HuZAF and HuAF2, respectively. In contrast, the VH domain of HuAF2 (Nie-based) varied from the chimeric version in the CDRs as well as the FRs, as indicated by a relatively high value of 1.71 Å for the optimal r.m.s. deviation over the entire VH. The comparable r.m.s. deviation in the HuZAF/ChiAF2 comparison is a more reasonable 0.85 Å. The crowding and collisions observed for the three HCDRs in the HuAF2 structure were eliminated in the HuZAF VH. By computer-assisted superpositioning with the program *O* (Jones *et al.*, 1991), the HuZAF VH-VL combination was found to be a nearly perfect fit to the chimeric structure (see also Table 2).

3.4. Comparison of the crystal packing in the HuZAF orthorhombic and monoclinic forms

Before exposure to IFN-γ, the monomeric HuZAF Fab crystallized in the orthorhombic $P2_12_12_1$ space group, with unit-cell parameters similar to those in crystals of the ChiAF2 and HuAF2 Fabs. The crystal-packing scheme for the orthorhombic form of the HuZAF Fab is illustrated in Fig. 4. In the crystal lattice, ribbons of indefinite length were produced by bilateral extended β-pleated sheets across adjacent Fab molecules. Hydrogen bonds were formed between parallel outermost β-strands, one consisting of residues 159–163 (designated as β-strand 4–4) in the CL domain (Fab molecule 1) and the second composed of residues 209–214 (β-strand 3–3) in the CH1 domain from a symmetry-related Fab (molecule 2). These interactions were repeated in reverse on the opposite side of the Fab (*i.e.* the β-strand 3–3 of CH1 Fab molecule 1, with the CL β-strand 4–4 on a third Fab molecule). In addition, the ε-amino group of Lys210H in each Fab was hydrogen bonded with the carbonyl O atom of the main chain of Ser54H in another molecule.

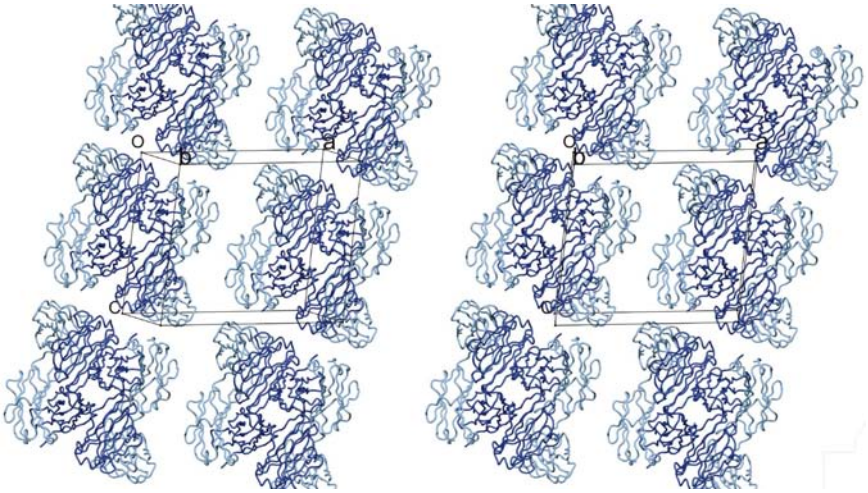

Figure 5
Packing of the HuZAF Fab in the monoclinic *C*2 space group. A loop consisting of residues 133–140 in CH1 was found to have changed its conformation and interlocked with a comparable loop to produce an asymmetric unit consisting of the two Fab molecules. The conformations of the L3-3 and H4–4 β-strands responsible for the packing of the orthorhombic form depicted in Fig. 4 were not altered when the HuZAF Fab crystallized in the *C*2 space group. However, their propensities for participating in dominant packing interactions were clearly subordinated to the tendencies of the altered CH1 loops of residues 133–140 to produce an interlocking dimer.

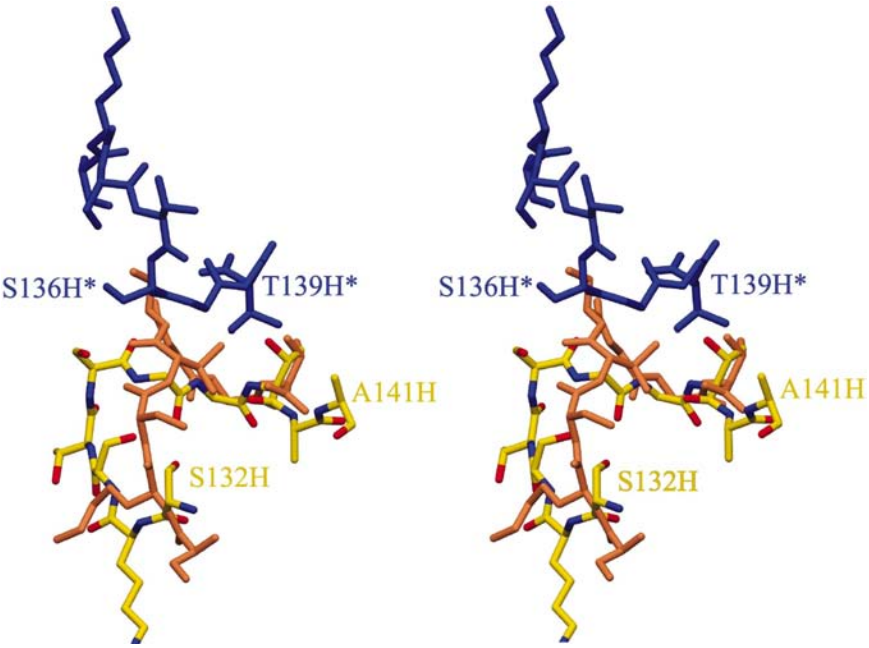

Figure 6
Comparison of the conformations of the loops of residues 132–140 in the orthorhombic and monoclinic forms. In the dimer (*C*2 monoclinic form), the loops are represented by yellow (O and N atoms colored red and blue) and blue. Residues in the second molecule of the asymmetric unit are marked with an asterisk. The model of the loop in the orthorhombic form is salmon-colored. Four residues (Ser136H, Gly137H, Gly138H and Thr139H) line each of the interacting surfaces of the two interlocked CH1 domains. If unaltered prior to crystallization, the Ser-Gly-Gly portion of the loop would invade the space of the blue model and thus be sterically incompatible with the dimerization interaction.

Comparisons of the contents of the two crystal forms revealed significant differences in the conformations of CH1 domains, rather than expected changes in the V domains. In the *C*2 space group, there are eight molecules of HuZAF Fabs in the unit cell, arranged in pairs. As shown in Figs. 5 and 6, loops composed of residues 133–140 in the H chains of the two Fabs in the *C*2 form were interlocked in antiparallel fashion to produce the asymmetric unit.

The amino-acid sequence of each CH1 packing loop interlocked with its counterpart in the second Fab is Lys-Ser-Thr-Ser-Gly-Gly-Thr-Ala. After Lys133H the residues were small and well suited for bestowing exaggerated flexibility on the loop. In one Fab molecule of the asymmetric unit, the electron density was broken for residue 134H and in the second residue 136H was problematical. However, it was difficult to build the 134H–136H tripeptide segments (Ser-Thr-Ser) any other way. Thr135H, Ser136H, Gly137H and Gly138H were located at the crest of the broad loop and were responsible for the observed changes in direction. In the $P2_12_12_1$ structure, this loop appeared to be markedly different in conformation, with the uncertainty that residues 134–136 were not well defined in this model either. We concluded that the malleability of the packing loop was the key to the conversion from the $P2_12_12_1$ to the *C*2 arrangement.

These interactions between the close-fitting antiparallel loops of residues 133–140

precluded the formation of extended β-pleated sheets found in the packing of HuZAF monomeric Fab molecules in the $P2_12_12_1$ space group. In the $C2$ form, both the CL and CH1 segments involved in the latter type of packing were in conformations suitable for β-strand pairing. However, they were prevented from doing so by the presence of two overhanging parallel segments (residues H1–12 and residues H107–115) from another VH domain, plus the loop L38–44 of the VL domain in a symmetry-related molecule.

In additional $C2$ packing patterns, the active site of each Fab in the asymmetric unit was juxtaposed head-to-head across a crystallographic dyad with the active site in a symmetry-related Fab. There was obviously no room to place an IFN-γ dimer between these two binding sites.

3.5. Local conformational changes in the active site of the monoclinic form of the HuZAF Fab

In the active site of the $C2$ form of the HuZAF Fab, there were two regions that showed conformational changes when compared with the orthorhombic Fab structure. The largest differences in position, required to avoid collision, were observed for Phe100H and Trp103H. Smaller movements of Leu101H and Phe104H accompanied the major shifts. Even more minor displacements were observed at Ala105H, but not at Asp106H. In the following position, Trp107H closely superimposed on its counterpart in the $P2_12_12_1$ structure. Comparisons of the HCDR3 segments in the two structures are shown in Fig. 7.

In the second locus immediately adjacent to HCDR3, Trp33H of HCDR1 in the $C2$ form occupied space assigned to Arg50H of HCDR2 in the orthorhombic structure. Its new position was in the interdomain space next to Tyr94L (CDR3) of the L chain. The tripeptide segment consisting of Tyr94L, Pro95L and Phe96L assumed a different orientation in the *C2* form. These structural relationships are illustrated in Fig. 8.

In summary, the conformational changes in the HUZAF Fab were concentrated in a zone heavily populated with accessible large side chains in HCDR3 and HCDR1. From this epicenter, progressively smaller

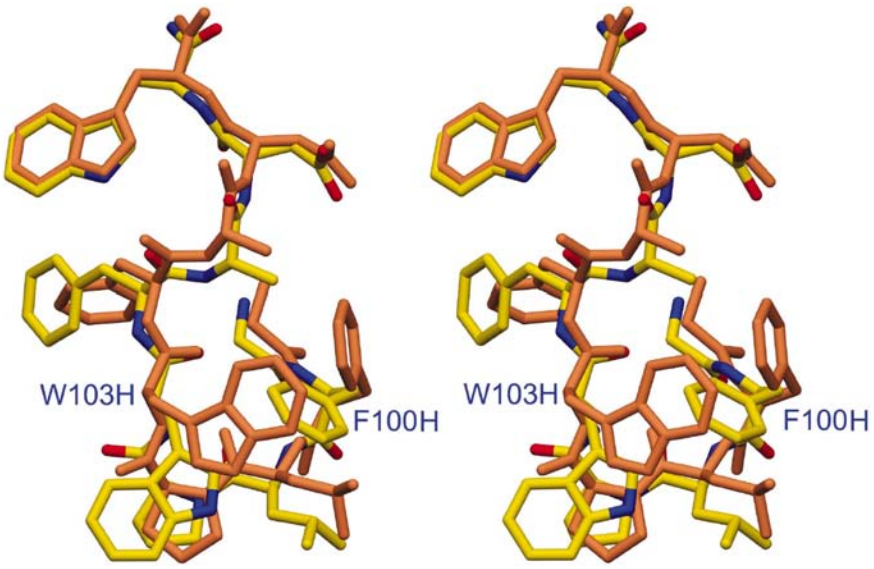

Figure 7
Stereo diagram of skeletal models of HCDR3 of the monoclinic ($C2$) and orthorhombic ($P2_12_12_1$) forms of the HuZAF Fab. The $C2$ variant is colored yellow, with the O atoms in red and the N atoms in blue. The entire $P2_12_12_1$ model is salmon-colored. Note that the greatest differences are in the Phe100H and Trp103H residues at the crest of the loop. In the $C2$ form, we propose that the movements could be explained by the recoil of Phe100H, with accentuated knock-on effects to Trp103H. Smaller concerted displacements were observed for Leu101H (lower right) and Phe104H (above Trp103H on the left). The chain reaction dissipated after Phe104H and ceased entirely by position 106 (Trp at top left).

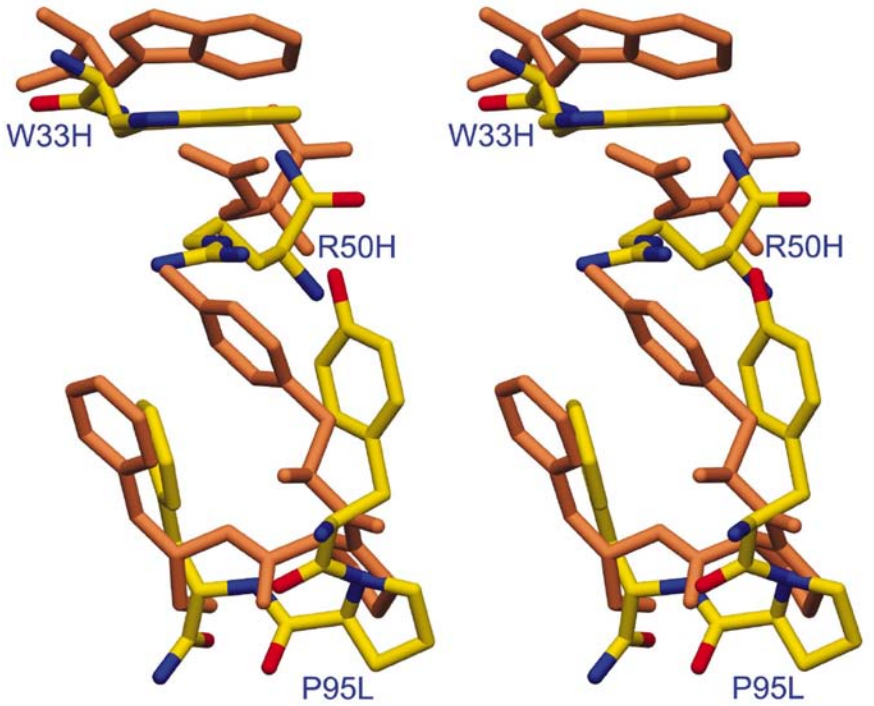

Figure 8
Stereo diagram of the orientations of key CDR components in the monoclinic ($C2$) and orthorhombic ($P2_12_12_1$) forms of the HuZAF Fab. Trp33H is from HCDR1, Arg50H is from HCDR2 and the tripeptide segment of Tyr94L (unlabeled, below 50H), Pro95L and Phe96L (unlabeled, to left of 95L) are from LCDR3. Coloring is similar to Fig. 7. In the monoclinic form, there is a chain reaction of induced conformational changes. Perturbation of Trp33H is propagated from one heavy chain CDR loop to another (Arg50H) and then across to the light chain (Tyr-Pro-Phe, residues 94–96).

displacements were noted in HCDR2 and across the channel in the L chain CDR3.

4. Discussion

4.1. Effect of framework choice on conformation of humanized antibodies

Relative to the chimeric Fab (ChiAF2), the HuAF2 Fab reported previously (Fan *et al.*, 1999) had VH CDRs that were confined to more congested local environments. These alterations presumably occurred as a result of adverse conformational changes that propagated from FR1 to CDR1. A single VH substitution of serine for Pro7 allowed the generation of antiparallel β-strand pairing of FR1 residues 5–8 with residues 19–22. This interaction led to compression of CDR1 from a 3_{10}-helix to an α-helix. Since CDR1 occupies a central location between CDRs 2 and 3, alterations in CDR1 affected the shapes of both its neighbors. Collectively, the antigen-contact residues were displaced from their relative positions and orientations in the active site of the ChiAF2 Fab. The structures reported here for HuZAF are much closer to that of the ChiAF2 Fab, whose V-domain sequences are entirely derived from the original mouse Ab. Thus, this best-sequence-fit-based design for HuZAF largely reversed the structural deficiencies present in HuAF2, whose VH framework sequences are less optimally matched to those of the mouse VH (Fig. 1). It is tempting to speculate that these differences in conformation may explain the higher level of biological activity of HuZAF relative to HuAF2. However, one should be aware of the observation that amino-acid changes in the HuZAF sequence at positions 11 (Leu to Val), 38 (Lys to Arg) and even 150 (Phe to Leu or Ala) in the constant domain are sufficient, individually or in concert, to cause significant reductions in the biological potency of the resulting Ab (Landolfi *et al.*, 2001), indeed to a level equivalent to that of Nie-based HuAF2.

With these caveats in mind, it is still evident that the CDR conformations in the HuZAF structures are much closer to those of the ChiAF2 than are those of HuAF2. Also, HuAF2 has a Val at critical position 11 of the VH and thus its structure provides some insight into the role of Val or Leu at this position. Defining the structural basis of the involvement of VH residue 38 in the neutralization capabilities of the HuZAF antibody is not straightforward because its side chain is well removed from both the junction of VH and CH1 domains and from the active site. Arg is generally a more prevalent occupant of position 38 than Lys in human VH domains. However, Lys38 is found in other AF2-derived molecules and apparently is also more desirable than Arg in the HuZAF variant.

Closer examination of the region around amino acid 11 of VH in each of the five structures (chimeric, HuAF2 and the three distinct HuZAF Fabs reported here) indicates some flexibility in the interaction of the terminal isopropyl group of amino acid 11 (C^{β}, $C^{\gamma1}$ and $C^{\gamma2}$ in Val; C^{γ}, $C^{\delta1}$ and $C^{\delta2}$ in Leu). In Fabs with Leu11, the distance from C^{γ} in Leu11 to C^{ζ} in Phe150 ranged from 4.4 Å (very close packing) in the orthorhombic HuZAF to 5.7 Å in the ChiAF2. The equivalent distance from Val11 to Phe150 in HuAF2 is an intermediate 4.9 Å. Thus, a simple distance-packing argument does not readily distinguish the structures of the more biologically active Abs. Our current working hypothesis is that the alterations in this so-called ball-and-socket region induce differences in flexibility that are important for the biological activity, but not necessarily for the binding affinity of these variants of the AF2 antibody.

4.2. Conformational changes in the HuZAF Fab in crystals grown from solutions of antigen–antibody complexes

Two general types of conformational changes were evident in the HuZAF structures in the monoclinic crystals. (i) The most noticeable effects occurred in CH1 residues 132–140, resulting in the formation of a packing dimer. (ii) A second set of changes occurred in the midst of the putative docking site for the antigen. This site was remote from regions associated with the crystal-packing interactions. Relative to the structure of the orthorhombic form of the HuZAF Fab, well defined deviations occurred in the orientations of closely spaced residues in HCDR3. These conformational shifts appeared to be propagated by ripple effects to adjacent regions in HCDR1 and HCDR2 and ultimately across domain boundaries to LCDR3.

5. Concluding remarks

The new structures reported in this paper and those described previously (Fan *et al.*, 1999) correspond to Fabs derived from antibodies with identical CDR sequences and, within a twofold range, similar affinities toward their antigen, IFN-γ. They thus represent a unique opportunity to evaluate not only the structural consequences of engineering their variable domains from mouse to human (Holmes & Foote, 1997), but also to consider the effects of two distinct strategies for framework choice in their VH domains.

The original descriptions of antibody humanization work based on the CDR-grafting strategy paid no special consideration to the choice of human framework-acceptor sequences (Riechmann *et al.*, 1988). Shortly after, Queen and coworkers suggested using a best-sequence-fit approach for framework choice in antibody humanization as a component of their general method (Queen *et al.*, 1989). Subsequent work demonstrated that such choice alone often determined the degree to which a rodent antibody could be humanized successfully (Gorman *et al.*, 1991; Singer *et al.*, 1993). Nonetheless, certain Ab humanizations based on a pre-determined sequence-independent choice of human framework sequences can be achieved successfully (Carter *et al.*, 1992; Tsurushita & Vasquez, 2003).

Here, we show that for the AF2 series of antibodies, HuZAF, the VH domain of which was designed using the best-sequence-fit approach, is significantly closer structurally to its mouse precursor than is the HuAF2 version. In the latter, VH was constructed using a human sequence with a lower

homology to the original mouse sequence (Fig. 3; Table 2). Thus, we present direct structural evidence in support of the approach of using best-matched frameworks, adding to previous evolutionary arguments (Kirkham *et al.*, 1992) and the results of biological and biochemical evaluation (Gorman *et al.*, 1991; Singer *et al.*, 1993) of distinctly engineered antibodies, which also favored use of the best-fit strategy.

This work was supported by grant HR00-093 to Paul Ramsland and Allen B. Edmundson, and OARS grant AR01.2-017 to ABE from the Oklahoma Center for Advancement of Science and Technology (OCAST) Research and Development Programs Division. For the early stages of this work, we also gratefully acknowledge the support of grant CA72803 from the National Cancer Institute, Department of Health and Human Services. We thank Dr Christina Bourne for advice and numerous discussions and Mrs Natalie Fessler and Mrs Joie White for preparing the manuscript.

References

Boulianne, G. L., Hozumi, N. & Shulman, M. J. (1984). *Nature (London)*, **312**, 643–646.
Brünger, A. T., Adams, P. D., Clore, G. M., DeLano, W. L., Gros, P., Grosse-Kunstleve, R. W., Jiang, J.-S., Kuszewski, J., Nilges, M., Pannu, N. S., Read, R. J., Rice, L. M., Simonson, T. & Warren, G. L. (1998). *Acta Cryst.* D**54**, 905–921.
Carter, P., Presta, L., Gorman, C. M., Ridgway, J. B., Henner, D., Wong, W. L., Rowland, A. M., Kotts, C., Carver, M. E. & Shepard, H. M. (1992). *Proc. Natl Acad. Sci. USA*, **89**, 4285–4289.
Collaborative Computational Project, Number 4 (1994). *Acta Cryst.* D**50**, 760–763.
Edelman, G. M. & Gall, W. E. (1969). *Ann. Rev. Biochem.* **38**, 415–466.
Fan, Z. C., Shan, L., Goldsteen, B. Z., Guddat, L. W., Thakur, A., Landolfi, N. F., Co, M. S., Vasquez, M., Queen, C., Ramsland, P. A. & Edmundson, A. B. (1999). *J. Mol. Recognit.* **12**, 19–32.
Fitzgerald, P. M. D. (1988). *J. Appl. Cryst.* **21**, 273–278.
Gorman, S. D., Clark, M. R., Routledge, E. G., Cobbold, S. P. & Waldmann, H. (1991). *Proc. Natl Acad. Sci. USA*, **88**, 4181–4185.
Gottlieb, P. D., Cunningham, B. A., Rutishauser, U. & Edelman, G. M. (1970). *Biochemistry*, **9**, 3155–3616.
Holmes, M. A. & Foote, J. (1997). *J. Immunol.* **158**, 2192–2201.
Johnson, S., Oliver, C., Prince, G. A., Hemming, V. G., Pfarr, D. S., Wang, S. C., Dormitzer, M., O'Grady, J., Koenig, S., Tamura, J. K., Woods, R., Bansal, G., Couchenour, D., Tsao, E., Hall, W. C. & Young, J. F. (1997). *J. Infect. Dis.* **176**, 1215–1224.
Jones, T. A., Zou, J. Y., Cowan, S. W. & Kjeldgaard, M. (1991). *Acta Cryst.* A**47**, 110–119.
Kirkham, P. M., Mortari, F., Newton, J. A. & Schroeder, H. W. Jr (1992). *EMBO J.* **11**, 603–609.
Kraulis, P. J. (1991). *J. Appl. Cryst.* **24**, 946–950.
Landolfi, N. F., Thakur, A. B., Fu, H., Vasquez, M., Queen, C. & Tsurushita, N. (2001). *J. Immunol.* **166**, 1748–1754.
Laskowski, R. A., MacArthur, M. W., Moss, D. S. & Thornton, J. M. (1993). *J. Appl. Cryst.* **26**, 283–291.
Maloney, D. G., Grillo-Lopez, A. J., White, C. A., Bodkin, D., Schilder, R. J., Neidhart, J. A., Janakiraman, N., Foon, K. A., Liles, T. M., Dallaire, B. K., Wey, K., Royston, I., Davis, T. & Levy, R. (1997). *Blood*, **90**, 2188–2195.
Matthews, B. W. (1968). *J. Mol. Biol.* **33**, 491–497.
Morrison, S. L., Johnson, M. J., Herzenberg, L. A. & Oi, V. T. (1984). *Proc. Natl Acad. Sci. USA*, **81**, 6851–6855.
Murshudov, G. N., Vagin, A. A., Lebedev, A., Wilson, K. S. & Dodson, E. J. (1999). *Acta Cryst.* D**55**, 247–255.
Navaza, J. (1994). *Acta Cryst.* A**50**, 157–163.
Otwinowski, Z. & Minor, W. (1997). *Methods Enzymol.* **276**, 307–326.
Ponstingl, H., Schwarz, J., Reichel, W. & Hilschmann, N. (1970). *Z. Physiol. Chem.* **351**, 1591–1594.
Queen, C., Schneider, W. P., Selick, H. E., Payne, P. W., Landolfi, N. F., Duncan, J. F., Avdalovic, N. M., Levitt, M., Junghans, R. P. & Waldmann, T. A. (1989). *Proc. Natl Acad. Sci. USA*, **86**, 10029–10033.
Riechmann, L., Clark, M., Waldmann, H. & Winter, G. (1988). *Nature (London)*, **332**, 323–327.
Rossmann, M. G. (1990). *Acta Cryst.* A**46**, 73–82.
Roussel, A. & Cambillau, C. (1989). *Silicon Graphics Geometry Partner Directory*, pp. 77–78. Mountain View, CA, USA: Silicon Graphics.
Singer, I. I. *et al.* (1993). *J. Immunol.* **150**, 2844–2857.
Thakur, A. B. & Landolfi, N. F. (1999). *Mol. Immunol.* **36**, 1107–1115.
Tsurushita, N. & Vasquez, M. (2003). *Molecular Biology of B Cells*, edited by M. Neuberger, pp. 533–546. New York: Academic Press.
Vincenti, F., Kirkman, R., Light, S., Bumgardner, G., Pescovitz, M., Halloran, P., Neylan, J., Wilkinson, A., Ekberg, H., Gaston, R., Backman, L. & Burdick, J. (1998). *N. Engl. J. Med.* **338**, 161–165.
Waldmann, T. A. (1991). *Science*, **252**, 1657–1662.
Zilber, B., Scherf, T., Levitt, M. & Anglister, J. (1990). *Biochemistry*, **29**, 10032–10041.